Analysis and Modeling of an FFHC-Controlled DC–DC Buck Converter Suitable for Wide Range of Operating Conditions

Somnath Maity, *Member, IEEE*, and Y. Suraj

Abstract—To achieve the best optimized performance in terms of stability and dynamic behavior of power electronic converters, it is necessary to use a more advanced control technique and accurate mathematical model. This paper proposes a fixed-frequency hysteretic current (FFHC) controller that uses both sliding-mode control (SMC) technique and fixed-frequency current controller with a hysteresis band to achieve all properties of the variable structure controller. However, realizing such fixed-frequency sliding-mode controller using small-signal-averaged (SSA) model of the power converters and Utkin's equivalent control technique may not be valid for all conditions. We show that it can be applicable only when the fast-scale dynamics of the converter system is stable, which can be achieved successfully by analyzing the stability of the FFHC-controlled buck converter using Filippov method and Floquet theory. The regions of stability are then presented to show the domains of existence of nominal period-1 and higher periodic orbits in 2-D parameter space. We also demonstrate how to derive the equivalent control law from the modified tristate converter topology to design the controller. Finally, the experimental results are presented to validate the effectiveness of this hybrid FFHC controller.

Index Terms—DC–DC buck converter, discontinuous systems, fixed-frequency hysteretic current (FFHC) control, multiscale oscillation, sliding-mode control (SMC), sliding motion (SM).

I. INTRODUCTION

OBTAINING accurate mathematical models for DC–DC converters and optimizing their performances over wide operating conditions, especially, for next-generation microprocessors [1], [2], are a challenge for power electronics design engineers. In recent years, much effort has been devoted to this research area, and reviews are now available on the subject [3], [4], and references therein. In most of cases, the methods of analysis are mainly based on constant-frequency pulse-width modulated (PWM) operation, standard linear controllers, and small-signal averaging techniques [3], [5]. The advantages of such methods include constant-frequency switching operation, well-established design methods, and many years of successful applications in practice. However, averaging is only an approximated procedure to obtain the low-frequency behavior of the actual switching model. The averaged model was found to fail in predicting many of the fast-scale instabilities that may develop in the voltage and current waveform at clock frequency result subharmonic oscillations and chaotic behavior [6], [7]. This shortcoming is due to the elimination of discontinuous effect of the real converter system and ignoring the microscopic dynamics inside the switching cycle [8]. Because of this approximation, the traditional use of averaging technique and also linear controller cannot always extract the best optimized performances over wide operating conditions [9]. It is, therefore, of great importance to be able to analyze and predict such instabilities to extract the best-optimized performance in terms of stability and dynamic behavior of power electronic converters.

It has, however, been recently reported that the performance of a power converter can be significantly improved by combining the different mode of controllers like sliding and constant-frequency PWM voltage-mode or current-mode controller [10]–[16]. As a result of this combination, the SMC essentially utilizes a constant-frequency switching control law to drive the state trajectory from any initial position onto a specified surface in the state space called the sliding or switching surface (SS), and maintain it on this surface for all subsequent time [17]. The main features of this sliding mode are the robustness against the load and the input voltage fluctuations. However, despite these unique advantages, most of the controllers reported on earlier are impractical for power converters because they either require complicated control circuitries and cost more [10]–[12], they are variable-frequency controllers [18], or they have a slow dynamical response [13], [14]. Moreover, they rely completely on smooth averaged models of the power converters and the control is only valid on a reduced-order SS.

With these issues in mind, we propose in this paper a hybrid FFHC controller, which is implemented on the basis of SMC technique and FFHC-mode controller with a hysteresis band. The choice of this variable structure controller is quite logical for power converters because the control and plant are both discontinuous. It retains all of the properties of an ideal SMC; that is, simplicity in design and practical realization, good dynamic response, and less overshoot in the regulated output voltage. In addition, it inherently acts as a current limiter to protect the converter from overloads, provides relatively larger bandwidth by eliminating compensating ramp signal, and reduces the impact of very high frequency dynamics due to parameter uncertainties on the closed-loop system.

However, it has been seen that the sliding motion (SM) of hybrid discontinuous systems (HDSs) can be successfully determined by using the notion of Utkin's equivalent control or Filippov continuation method [19]. For single discontinuous SS, there exists a unique solution of equivalent dynamics and the SM obtained from these methods are the same. However, with boundary layer control, the SM only exists when the fast-scale dynamics are stable. The mathematical proof of this concept has already been developed earlier in multiscale HDSs [20]. Since the power electronic converters come under this class of systems [21]–[23], the equivalent equation of motion derived from Utkin theory may not be successful always in predicting the existence of a unique solution [20]. It can only be successfully used when the long-time averaging of fast-scale oscillations become zero, in other words, when the fast-scale oscillations of the inductor current and the capacitor voltage ripple of the converter are periodic. It is, therefore, necessary to predict fast-scale instability margin for designing the SMC power converters based on Utkin's theory.

In this paper, we apply this concept and design the FFHC-controlled tristate dc–dc buck converter for extracting its best optimized performance, i.e., fast transient response without fast-scale instability under wide range of line and load variation. The paper is organized as follows. Section II revisits the condition of SM in an HDS with single and multiple SSs. In Section III, we describe the proposed system and its mathematical model. We then illustrate how Utkin's equivalent control law and Filippov's method together can be used to design this converter system and to extract its best optimized performance. Finally, in Section V, the performance of the proposed scheme is experimentally verified and compared with the classical peak current-mode-controlled buck converter without slope compensation.

II. Sliding-Motion in a Discontinuous System

From dynamical system [24], or from control theory point of view [17], the HDSs with right-hand side discontinuity can be described as

$$\frac{dx}{dt} = f(x) = \begin{cases} f_1(x); \ x \in R_1 & \text{if } h(x) < 0 \\ f_2(x); \ x \in R_2 & \text{if } h(x) > 0 \end{cases} \quad (1)$$

where $R_{1,2}(x) \in \Re^2$ are the smooth regions separated by 1-D discontinuous switching hypersurface $h(x)$. The systems are called continuous switching if $f_1(x) = f_2(x)$ at any point of the boundary $\Sigma_{1,2}$ separating two adjacent regions R_1 and R_2, and the vector $\dot{x}$ is uniquely defined at any point of the state space and trajectories in region R_1 approaching transversally the boundary $\Sigma_{1,2}$, cross it and then enter into the adjacent region R_2. By contrast, in discontinuous systems (called Filippov systems), two different vectors $\dot{x}$, namely $f_1(x)$ and $f_2(x)$, can be associated to a point $x \in \Sigma_{1,2}$. If the transversal components of $f_1(x)$ and $f_2(x)$ have the same sign, the trajectory crosses the boundary and has at that point a discontinuity in its tangent vector. On the contrary, if the transversal components of $f_1(x)$ and $f_2(x)$ are of opposite sign, i.e., if the two vector fields are pushing in opposite directions, the state of the system is forced to remain on the boundary and slide on it. Although, in prin-
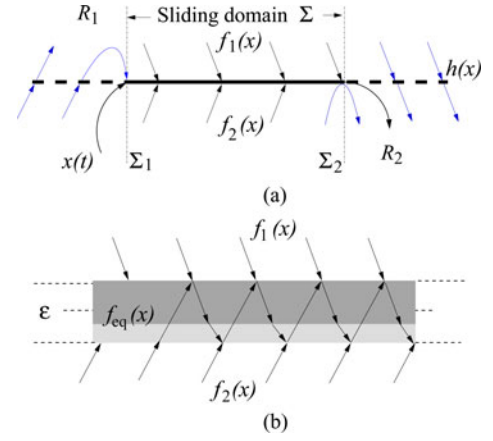

Fig. 1. A representative diagram showing (a) the direction of both piecewise smooth vector fields $f_1(x)$ and $f_2(x)$ for an SM on an ideal SS $h(x)$, and (b) the direction of outside and inside vector fields for the ϵ-neighborhoods SS. ($f_{\text{eq}} \in (f_1(x), f_2(x), f_3(x))$.

ciple, motions on the boundary could be defined in different ways [19], the most natural one is Filippov convex method [24] which defines SMs on Σ as the solutions on $\Sigma_{1,2}$ of the continuous ordinary differential equation

$$\frac{dx}{dt} = F(x) = \alpha f_1(x) + (1 - \alpha) f_2(x) \quad (2)$$

where $F(x)$ is a convex combination of $f_1(x)$ and $f_2(x)$ tangent to $\Sigma_{1,2}$ at x, with a scalar function

$$\alpha = \frac{\partial h(x)/\partial x f_2(x)}{\partial h(x)/\partial x [f_2(x) - f_1(x)]} \in [0, 1].$$

Generically, this convex combination is unique. Thus, the state portrait of a Filippov system is composed of the sliding state portrait on Σ defined by boundaries $\Sigma_{1,2} = \{x \in h(x) : \alpha = 0, 1\}$ and of the standard state evolutions in each region $R_{1,2}$ as shown in Fig. 1(a).

However, in a real-life system, sliding mode actually occurs not on its discontinuity surface, but within the vicinity of that discontinuity or within a boundary layer surrounded by multiple switching surfaces (MSSs), for example, a hysteresis control. In such situations, the equivalent motion of the system along the single SS $h(x)$ is not defined as a continuous sense $\dot{x} = F(x)$. Here, the sharp transition of trajectories evolution from one mode $f_1(x)$ to another $f_2(x)$ does not occur at $h(x)$, rather the trajectories travel a farther distance of ϵ [see Fig. 1(b)]. The vector field $f_i(x)$ (where $i = 1, 2, 3$) remains constant until it reaches the boundary. Once it hits the boundary, it bounces off and returns to interior of boundary layers. Thus, trajectories chatter back and forth across the SSs. We consider the "chattered box" as infinitesimally small, i.e., $\epsilon \to 0$. If the chattering dynamics inside ϵ occurs rapidly compared to natural time scale of the SS, it is reasonable to consider two separate time scales, the chattering scale and the other natural time scale, of the field. Then, the equivalent dynamics inside the chattering box is the average of the impinging vector fields $f_1(x)$, $f_2(x)$, and $f_3(x)$, weighted by the proportion of the time flow spent in each mode

which is given as

$$\frac{dx}{dt} = f_{\mathrm{eq}}(x) = \alpha_1 f_1(x) + \alpha_2 f_2(x) + \alpha_3 f_3(x) \qquad (3)$$

where $\alpha_1, \alpha_2, \alpha_3 \geq 0$, and $\alpha_1 + \alpha_2 + \alpha_3 = 1$. Thus, to ensure the existence of a unique solution of the SM of (3), the trajectories as a set must be tangent to the SS [25]. This can only happen when the long-time averaged values of coefficients α_1, α_2, and α_3 become constant [20], [25]. These coefficients are known as the Fillipov coefficients. Once these coefficients are well defined, there will not be any transversal components of the average vector field $f_{\mathrm{eq}}(x) \in (f_1(x), f_2(x), f_3(x))$ along the SS. We can write this transversal condition mathematically as

$$\frac{\partial h(x)}{\partial x} f_{\mathrm{eq}}(x) = 0. \qquad (4)$$

Here, it is important to note that (4) is inherently the same as the SM determined from the Utkin's equivalent control [17] for single discontinuous SS. Where the dynamics are essentially determined by replacing the discontinuous control input u by an equivalent control u_{eq}, given by the solution of $\frac{dh(x)}{dt} = 0$ or $\frac{\partial h(x)}{\partial x} f_{\mathrm{eq}}(x, u_{\mathrm{eq}}) = 0$, if such a solution exists. When the state-space dynamic is expressed in the form $\frac{dx}{dt} = Ax + Bu + D$, the equivalent control may be explicitly calculated by

$$u_{\mathrm{eq}} = -\left[\frac{\partial h(x)}{\partial x} B\right]^{-1} \frac{\partial h(x)}{\partial x} [Ax + D] \qquad (5)$$

where $\frac{\partial h(x)}{\partial x} B$ should be a nonsingular square matrix. Substituting (8) into (7), we get the equivalent dynamics

$$\dot{x} = Ax - B\left[\frac{\partial h(x)}{\partial x} B\right]^{-1} \frac{\partial h(x)}{\partial x} [Ax + D]. \qquad (6)$$

Therefore, a solution is an absolutely continuous vector-valued function, which outside the surfaces satisfies (1), and on and inside their boundaries satisfies (6) for almost all t, as mentioned before.

III. MODELING OF AN FFHC-CONTROLLED DC-DC BUCK CONVERTER

The schematic diagram of an FFHC-controlled tristate buck converter is shown in Fig. 2(a). It consists of an inductor L, a capacitor C, a load resistance R, a conduction loss series resistance r, an uncontrollable switch D, and two controllable switches Q_1 and Q_2. The switching of the Q_1 and Q_2 are controlled by the FFHC control logic.

A. Controller Architecture and Switching Logic

The controller architecture needed to achieve such switching logic circuit is implemented by means of a nested feedback controller. The slow outer voltage controller is used to generate the quasi-stationary boundary layers [25] of the hysteresis loop. This is achieved by obtaining the equivalent reference current signals i_{ref}^+ and i_{ref}^- as a linear combination of the output capacitor voltage v and a reference voltage V_{ref} in the form

$$i_{\mathrm{ref}}^+ = k_p(V_{\mathrm{ref}} - v), \quad \text{and} \quad i_{\mathrm{ref}}^- = i_{\mathrm{ref}}^+ - \Delta \qquad (7)$$
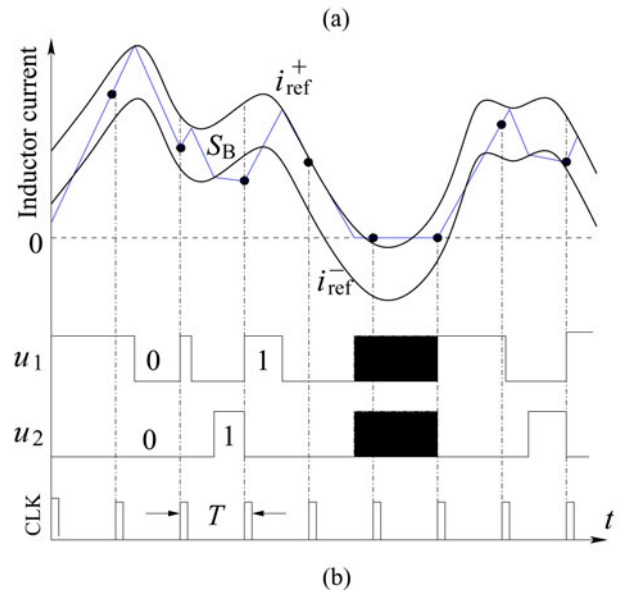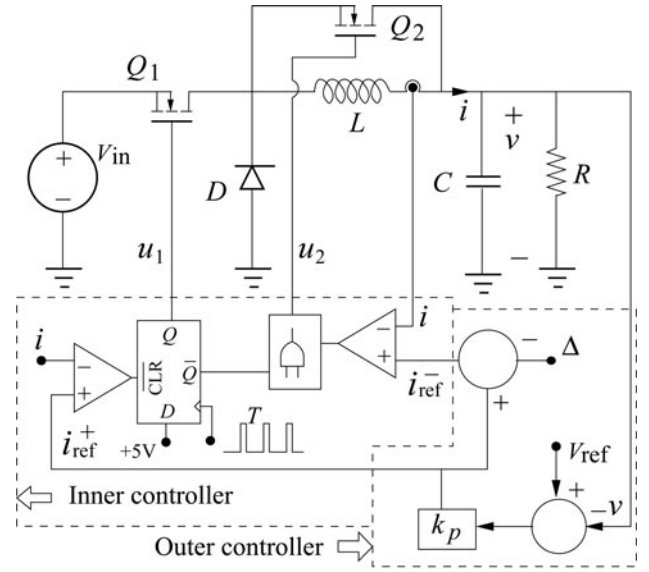

Fig. 2. (a) Schematic diagram of the FFHC-controlled tristate buck converter. (b) Generation of binary switching signals u_1 and u_2 in a switching box S_B. The black region indicates where switches Q_1 and Q_2 are turned OFF.

where k_p is the gain of the proportional controller and Δ is the bandwidth between i_{ref}^+ and i_{ref}^-. While the fast inner current controller is used to generate the binary control signal $u \in (0, 1)$ where $u = (u_1 \ u_2)^T$, by comparing the sensing inductor current i with two threshold reference currents $i_{\mathrm{ref}}^+, i_{\mathrm{ref}}^-$ and an externally generated clock pulse of time period T. The combination of these three signals eventually forms a bounded chattered box simply called the switching box

$$S_B = \{(i, v) : i_{\mathrm{ref}}^- \leq i \leq i_{\mathrm{ref}}^+, t < T\} \in \Re^2 \qquad (8)$$

for this converter system. Depending on the initial position of the inductor current $i(0)$, the converter may operate into two modes: one when the inductor current i is outside the boundary layers and the other when it is inside. At the beginning of every switching cycle, we determine whether the inductor current
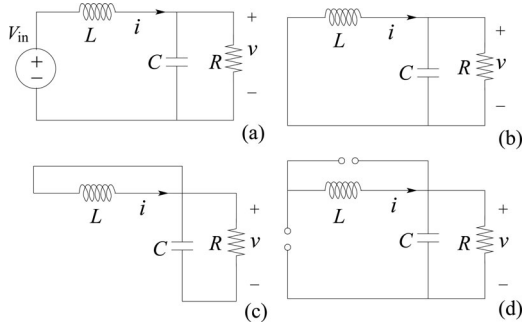
Fig. 3. Circuit configurations of a tristate buck converter during different modes of operation: (a) M_1. (b) M_2. (c) M_3. (d) M_4.

Fig. 4. Switching flow diagram of tristate hysteretic current-controlled buck converter.

$i|_{t=T}$ is within the boundary of S_B or not. If it is inside, at the start of the clock period, the switch Q_1 is turned ON and Q_2 is turned OFF, then the inductor current i raises. When i reaches a peak value i_{ref}^+, the Q_1 is turned OFF. The inductor current i starts falling until it reaches the lower threshold current i_{ref}^-. The switch Q_2 is turned ON when i reaches i_{ref}^- and remains ON until the arrival of the next clock pulse. If i reaches the next clock pulse with a nonzero value without intersecting i_{ref}^-, the operation is said to be in continuous conduction mode (CCM), otherwise it is in pseudocontinuous conduction mode (PCCM) [26]. But, if i reaches zero value before the next clock cycle, the switch D is turned OFF, and then the operation is said to be in discontinuous conduction mode (DCM). This mode of operation occurs when the boundary layer currents i_{ref}^+ and i_{ref}^- [from (7)] become negative.

However, if the inductor current $i|_{t=T}$ is outside of S_B, Q_1 is turned ON and Q_2 is turned OFF when $0 < i|_{t=T} < i_{\mathrm{ref}}^-$ and both the switches are turned OFF when $i|_{t=T} > i_{\mathrm{ref}}^+ > 0$. But all three switches remain OFF throughout the clock period if $i|_{t=T} = 0$.

B. Converter Dynamics and Equations of SSs

There are four configurations as shown in Fig. 3, and described by four sets of differential equations, as follows:
M_1: When Q_1 is ON, Q_2 is OFF and D is in reverse bias, the system equation is

$$\frac{dx}{dt} = f_1(x) = A_1 x + B_1 \quad \text{for} \quad (u_1, u_2) = (1, 0) \quad (9)$$

M_2: When Q_1 is OFF, Q_2 is OFF and D is in forward bias, the system equation is

$$\frac{dx}{dt} = f_2(x) = A_2 x + B_2 \quad \text{for} \quad (u_1, u_2) = (0, 0) \quad (10)$$

M_3: When Q_1 is OFF, Q_2 is ON and D is in reverse bias, the system equation is

$$\frac{dx}{dt} = f_3(x) = A_3 x + B_3 \quad \text{for} \quad (u_1, u_2) = (0, 1) \quad (11)$$

M_4: When both Q_1 and Q_2 are OFF and D is in reverse bias, the system equation is
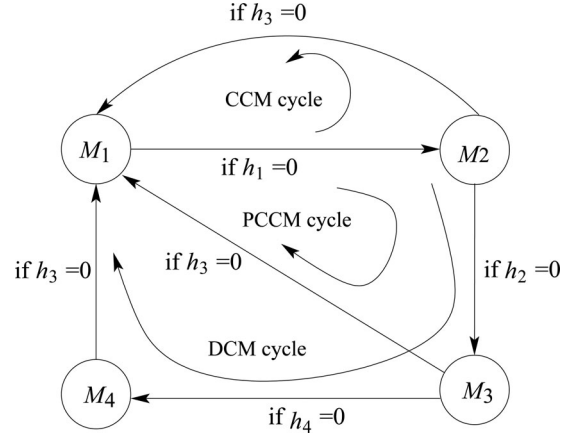
$$\frac{dx}{dt} = f_4(x) = A_2 x + B_4 \quad (12)$$

where

$$A_1 = A_2 = \begin{pmatrix} -1/RC & -1/C \\ 1/L & -r/L \end{pmatrix}$$

$$A_3 = \begin{pmatrix} -1/RC & 0 \\ 0 & -r/L \end{pmatrix}, \quad A_4 = \begin{pmatrix} -1/RC & 0 \\ 0 & 0 \end{pmatrix}$$

$$B_1 = \begin{pmatrix} V_{\mathrm{ref}}/RC \\ (V_{\mathrm{in}} - V_{\mathrm{ref}})/L \end{pmatrix}, \quad B_2 = \begin{pmatrix} V_{\mathrm{ref}}/RC \\ -V_{\mathrm{ref}}/L \end{pmatrix}$$

$$B_3 = B_4 = \begin{pmatrix} V_{\mathrm{ref}}/RC \\ 0 \end{pmatrix}, \text{ and } x = [(V_{\mathrm{ref}} - v) \quad i]^T$$

are the state variables. Here, the switching occurs whenever the solution of each subsystem (vector field) reaches the switching function specifically defined for that subsystem. The switching function between the subsystems M_1 and M_2 is given by

$$h_1(x) := i_{\mathrm{ref}}^+ - kx_2 = 0 \quad (13)$$

where k is the scaling factor. When x hits the boundary $h_1(x)$, switching occurs and subsequently the evolution of x is governed by the subsystem M_2. Three switching functions may exist when trajectories are in the subsystem M_2. One is the clock signal for resetting the switch that moves the system from M_2 to M_1 and the others are at $i = i_{\mathrm{ref}}^-$ and $i = 0$, which moves the system from M_2 back to M_1 through subsystem M_3, or from M_2 to M_1 through subsystems M_3 and M_4, respectively. These three functions can be described as

$$h_2(x) := kx_2 - i_{\mathrm{ref}}^- = 0 \quad (14)$$

$$h_3 := t - T = 0 \quad (15)$$

$$h_4 := x_2 = 0 \quad (16)$$

while in M_4 the system has only one switching function $h_3(x) := t - T = 0$. If the state hits $h_3(x)$, it returns to M_1. Since in each clock cycle the system may operate either in CCM, PCCM or DCM, the model can be represented by the switching flow diagram shown in Fig. 4. However, only dynamics of PCCM operation are presented here.
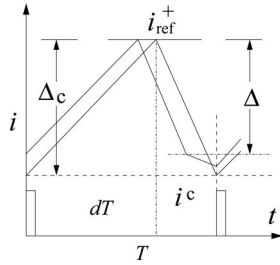
Fig. 5.   Inductor current at the edge of CCM operation.

Fig. 6.   A typical periodic trajectory evolution of the FFHC-controlled tristate buck converter within the switching box S_B for $L = 200\ \mu H$, $C = 100\ \mu F$, $r = 0.01\ \Omega$, $\Delta = 0.001$, $T = 2\ \mu s$, $k = 1$, $k_p = 5.5$, $V_{\rm ref} = 5$ V, $V_{\rm in} = 12$ V, and $R = 7.5\ \Omega$.

C. Critical Hysteresis Bandwidth Δ_c

In order to operate the converter in PCCM, we need to calculate first the critical hysteresis bandwidth Δ_c. Here, Δ_c is the boundary condition between two isolated converter topologies CCM and PCCM, respectively. If the inductor current ripple Δ is less than this critical value Δ_c, the converter operates in PCCM, otherwise it operates in CCM. Moreover, Δ_c can be defined as

$$\Delta_c = i_{\rm ref}^+ - i_c \tag{17}$$

where i_c is the Tth instant inductor current at the edge of CCM operation as shown in Fig. 5. Considering the initial position of state variables $x(dT) = \begin{bmatrix} V_{\rm ref} - V_o & i_{\rm ref}^+ \end{bmatrix}^T$ (V_o represents the steady-state dc output voltage) and solving the solution of subsystem (10) can be given as

$$x(T) = e^{A_2(1-d)T}x(dT) + \int_{dT}^{T} e^{A_2(T-\tau)}B_2\, d\tau \ \ \forall x \in M_2 \tag{18}$$

where d is the steady-state duty ratio, the critical inductor current i_c can be easily expressed as a function of ON/OFF switching instant inductor current $i(dT)$. However, since $x(T)$ in (18) is a function of matrix exponent $e^{A(1-d)T}$, one cannot find its exact explicit form of expression as a function of $i(dT)$. Based on first-order approximation, it can be expressed explicitly as

$$i_c = i_{\rm ref}^+ - \frac{r(1-d)T}{L}i_{\rm ref}^+ - \frac{d(1-d)T}{L}V_{\rm in} \tag{19}$$

where $i(dT) = i_{\rm ref}^+$, and $i_{\rm ref}^+$ is the upper boundary function defined by $i_{\rm ref}^+ = k_p(V_{\rm ref} - v)$. Further substitution of $i_{\rm ref}^+|_{t=dT} \approx k_p(V_{\rm ref} - dV_{\rm in})$ into (19), therefore, yields the critical condition

$$\Delta_c = \frac{rk_p(1-d)T}{L}V_{\rm ref} + \frac{d(1-d)T(1-rk_p)}{L}V_{\rm in}. \tag{20}$$

Here, the parameters r, L, T, and $V_{\rm ref}$ are known and k_p, $V_{\rm in}$, and d are unknown. Keeping $V_{\rm in}$ and all other parameters constant, from (20) we obtain the maximum current ripple Δ required for the PCCM operation which is at $d = 0.5$

$$\Delta = \frac{k_p rT}{2L}V_{\rm ref} + \frac{(1-rk_p)T}{4L}V_{\rm in}. \tag{21}$$

For every clock cycle, the value of Δ in (21) thus gives us the necessary condition for a successful converter operation in PCCM when state vectors evolve inside the boundary layers of S_B periodically. In 2-D state space, a representative periodic
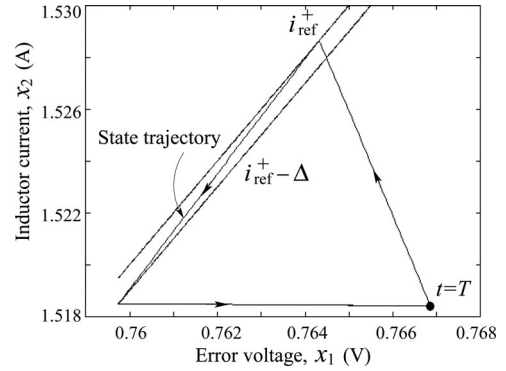
evolution of state trajectories and their corresponding boundary layers are shown in Fig. 6.

However, it is important to note that in each clock cycle, trajectories may evolve outside or inside boundary layers of S_B. For an arbitrary initial position $x(0)$, the controller

$$u = \begin{cases} \left.\begin{array}{ll} u_1^+ = 1, & h_1(x) < 0 \\ u_1^- = 0, & h_1(x) > 0 \end{array}\right\} \text{ if } x \text{ is outside} \\ u_{\rm eq} \in (u_1, u_2) \quad \text{ if } x \text{ is inside} \end{cases} \tag{22}$$

therefore drives the trajectories to reach S_B in finite time $t_s > 0$. Once this happens, a hysteretic flow inside the switching box starts and an equivalent motion continues to move toward the quasi-equilibrium point.

IV. SM AND SMC IN THE FFHC-CONTROLLED TRISTATE BUCK CONVERTER

The classical smooth equivalent control law (8) always approximates the dynamics due to MSSs. Because of this improper approximation, achieving a unique solution of real power electronic systems is not so straightforward. The systems having single SS or MSSs with $\Delta \to 0$ always have a unique solution [17], [24], whereas in multiscale power electronics systems, the unique solution only exits when the long-time averaging of fast-scale oscillations becomes zero (as explained in Section II). This zero average dynamics condition, however, can be obtained by analyzing the stability of a periodic orbit. There are three general approaches which are normally used to analyze fast-scale instability: 1) the Poincaré map [27], [28]; 2) the Floquet theory; and 3) the monodromy matrix using Filippov theory [29]. To apply this concept, we organize this section as follows. First, based on an ideal SS $h(x)$, the conditions for the existence of a sliding mode are found. Second, using monodromy matrix, the fast-scale stability analysis is performed and corresponding regions of different periodic orbits are identified for safe operating condition. Finally the equivalent equation of the motion is derived to design the controller accordingly.
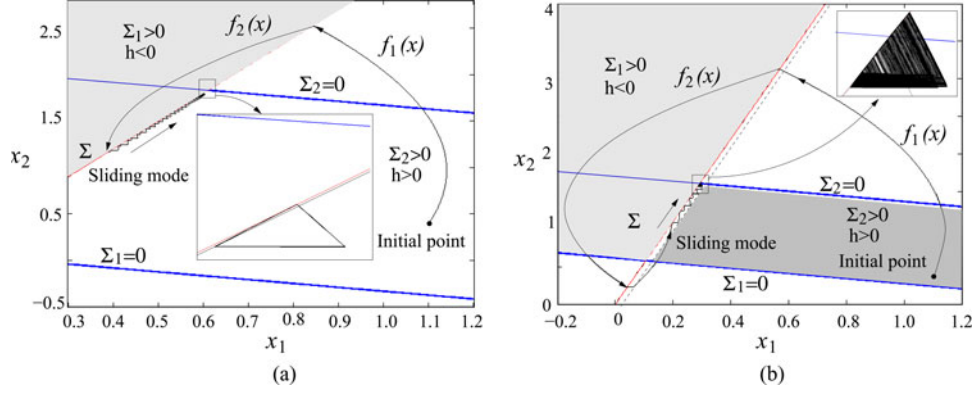
Fig. 7. Regions of existence of SM and state trajectories evolution of the FFHC-controlled tristate buck converter for (a) periodic mode of operation when $R = 8\ \Omega$, and (b) aperiodic mode of operation when $R = 4\ \Omega$. The other parameters are the same as shown in Fig. 6. The critical boundaries $\Sigma_{1,2}$ are obtained from (25) and (26).

A. Existence Conditions of ϵ-neighborhoods SSs

Assume there exist ϵ-neighborhoods SSs (where $\epsilon \to 0$), given by

$$h(x) = k_p x_1 - k x_2. \tag{23}$$

From Utkin theory [17], we know that an SM exists in the vicinity of an SS $h(x)$ if the following local reachability conditions $\lim_{h(x)\to0^-} \frac{dh(x)}{dt} > 0$, and $\lim_{h(x)\to0^+} \frac{dh(x)}{dt} < 0$, or $\lim_{h(x)\to0} \frac{dh(x)}{dt} h(x) < 0$ are simultaneously satisfied. The explicit form of such ϵ neighborhood reachability condition can be derived by simply substituting the time derivative of $h(x)$

$$\frac{dh(x)}{dt} = \frac{\partial h(x)}{\partial x} \frac{dx}{dt} = \begin{cases} J f_1(x) > 0 & \text{if } h(x) < 0 \\ J f_2(x) < 0 & \text{if } h(x) > 0 \end{cases} \tag{24}$$

into this condition, where $J = \partial h(x)/\partial x = [k_p - k]$. Replacing (9) and (10) into (24), and applying the control law (23), the existence region of SM or SMC can be expressed as

$$\Sigma_1 := -Mx_1 - Nx_2 + PV_{\text{ref}} - \frac{kV_{\text{in}}}{L} > 0 \quad \text{for } u_1^+ = 1 \tag{25}$$

$$\Sigma_2 := -Mx_1 - Nx_2 + PV_{\text{ref}} < 0 \quad \text{for } u_1^+ = 0 \tag{26}$$

where $M = \left(\frac{k}{L} + \frac{k_p}{RC}\right), N = \left(\frac{k_p}{C} - \frac{rk}{L}\right)$, and $P = \left(\frac{k}{L} + \frac{k_p}{RC}\right)$. The limiting boundaries (25) and (26) give the necessary region of existence for the SM on smooth SS [12], [30]. Here L, C, k, and V_{ref} are the known parameters and their exact values can be substituted directly into the aforementioned inequalities for inspection. However, for a range of V_{in} and R, it is necessary to consider the boundary points of these parameter values. The conformation of either the maximum or minimum point of these parameter values is generally sufficient for ensuring the abidance of the existence condition for the entire range of operation. Knowing the boundary points of V_{in} and R, and making the assumption that the controller is designed with a static SS to meet the existence conditions for steady-state operation. Therefore, it is possible to calculate the boundaries of proportional gain k_p as

$$0 < k_p < \frac{kRC}{L}\left(\frac{V_{\text{ref}}}{x_{1\text{ss}}} - 1\right) + \frac{krC}{L}\frac{V_{\text{ref}}}{x_{1\text{ss}}} \tag{27}$$

where the steady-state variables are $x_{\text{ss}} = [x_{1\text{ss}}\ x_{2\text{ss}}]^T$. The expressions (25)–(27) are essentially interpreted as a condition, requirement for the system trajectories to be oriented toward the SS, from both sides. Since the system trajectories are directed toward the $h(x)$, once they reach $h(x)$, they cannot leave it anymore and continue to slide along the SS toward the equilibrium, and this solution is unique. Is it valid in power electronic circuits with MSSs?

To explore this question, we numerically simulate the converter using MATLAB/SIMULINK for two different cases: one when converter operates in periodic mode, and the other when it operates in aperiodic mode. Based on approximate smooth SS $h(x) \approx 0$ and the inequality constraint (27), the region of existence of SM is identified and the state trajectories evolution are also captured (see Fig. 7). Here, the critical boundaries $\Sigma_{1,2}$ represent the conditions where vector field $f_1(x)$ or $f_2(x)$ is tangent to $h(x)$ and outside of $\Sigma_{1,2}$; the approaching trajectories on either side of SS, cross it transversely and enter into the adjacent region. On the contrary, inside the boundaries, both $f_1(x)$ and $f_2(x)$ are pushing in opposite direction, so the trajectories are forced to remain on $h(x)$ and start sliding along the surface. However, it is observed that the motion may or may not remain strictly inside the sliding segment Σ as $t \to \infty$ [see inset of Fig. 7(a) and (b)].

A closer look at the inner dynamics of state trajectories reveal that when the inductor current bounces off the edge of S_B and returns to the interior of S_B, the associated time fractions of vector field or duty ratios are well defined and the existence condition is satisfied. However, inside S_B, the converter may operate in different modes of operation, thereby it can also exhibit various kinds of nonlinear behaviors such as chaos, quasi-periodicity, and limit cycle oscillations [7]. Out of these nonlinear phenomena, there are two degenerate cases, quasi-periodicity and chaos, where the inductor current i inside S_B can either aperiodically oscillate and hit the corner of S_B [7] or move without hitting the corner points if it evolves on a torus. The dynamics are then characterized by the existence of two (or more) frequencies which are incommensurate [31], [32], and hence the duty ratios of the converter would not be well defined. In such situations, the existence conditions (25) and (26), which were originally
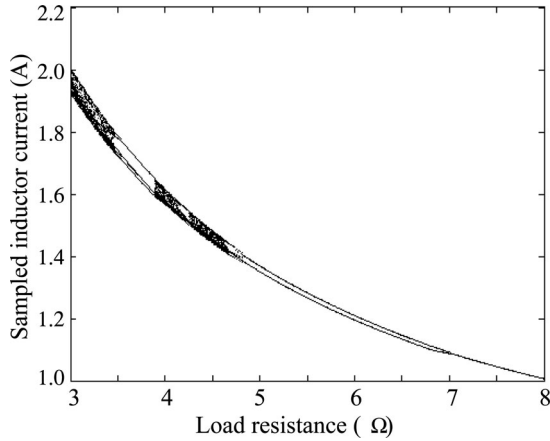
Fig. 8.   Bifurcation diagrams of sampled inductor current showing the mechanism of loss of stability of period-1 orbit when the converter is initially operated in PCCM region. The load resistance $R = (8–3)$ Ω is taken as the bifurcation parameter. All other parameter values are the same as shown in Fig. 6.
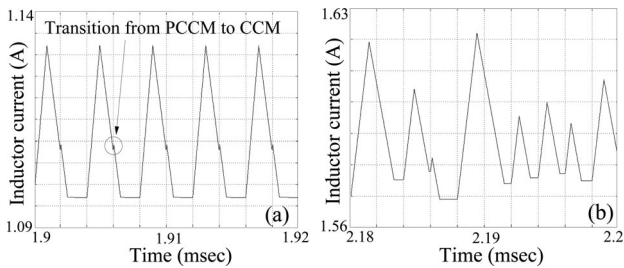

Fig. 9.   The continuous-time inductor current waveform showing (a) the direct transition from PCCM to CCM operation for $R = 6.83$ Ω, and (b) a typical chaotic oscillation for $R = 4.68$ Ω.

defined for single SS, are not always valid for deriving equivalent control law with MSSs. The representative bifurcation diagram of the FFHC-controlled buck converter is shown in Fig. 8, where the sampled inductor current is taken as the plotted variable. At high values of R, a stable period-1 orbit exists in PCCM. However, with a decrease in R, this orbit becomes unstable through a smooth period-doubling bifurcation at $R \approx 7.05$ Ω. Subsequently, one of the branches of the period-2 orbit hits the border between PCCM and CCM operation at $R \approx 6.83$ Ω as shown in Fig. 9(a). Available border collision bifurcation theory can successfully predict this direct transition from a periodic orbit to aperiodic orbit. As the parameter is further reduced, a series of smooth and border collision bifurcations occur in close succession, and finally it bifurcates into chaotic behaviors at $R \approx 4.68$ Ω. The continuous-time waveform of a typical chaotic inductor current oscillation at $R = 4$ Ω is shown in Fig. 9(b).

Thus, we can see that if the converter operates in PCCM, the existence conditions (25) and (26) derived for a ϵ-neighborhood of $h(x)$ can be successfully used only for a guaranteed reaching condition of trajectories into S_B, but not for the SM of that hysteretic flow inside.

B. Existence Region for Hysteretic Flow

In order to identify the existence region of the high-frequency hysteretic flow inside and to observe the stability status of the

converter system, it is necessary to estimate the fast-scale stability margin at the clock speed [23]. It is also necessary to estimate the range of external parameters that will ensure periodic operation without the onset of chaos. The sampled-data model (or Poincaré map) was addressed earlier [6], [27] to solve this problem. Even though it is conceptually simple, it yields complicated equations for most converters, and as a result, this approach has not found widespread acceptance among mainstream power electronic practitioners. The stability analysis using the fundamental solution matrix over a complete cycle or monodromy matrix, thus, provides an alternative method of obtaining the Jacobian of the Poincaré map when the nonlinear map cannot be explicitly derived.

The monodromy matrix is a composition of the state transition matrices for the pieces of the orbit that lie in the individual subsystems, and the saltation matrix can be expressed as [24], [33]

$$S = I + \frac{[f^+(x) - f^-(x)]\partial h(x)/\partial x}{\partial h(x)/\partial x \; f^-(x) + \partial h(x)/\partial t} \qquad (28)$$

where I is the identity matrix of the same order as that of number of state variables. When converter operates in PCCM, the state transition matrix over the complete cycle can then be composed of the state transition matrices over the three phases of evolution and three saltation matrices for the switching from M_1 to $M_2(S_1)$, from M_2 to the free-wheeling state $M_3(S_2)$, and finally switching back to $M_1(S_3)$ [34]

$$W = S_3 \Phi_3 S_2 \Phi_2 S_1 \Phi_1 \qquad (29)$$

where the state transition matrices Φ_1, Φ_2, and Φ_3 are obtained as matrix exponentials $e^{A_1 d_1 T}$, $e^{A_2 d_2 T}$, and $e^{A_3 d_3 T}$, respectively. In order to evaluate these, one needs to know the duty ratio d_1, d_2, and d_3. This can be obtained following [27] using the Newton–Raphson method. Alternatively, one can use any standard simulator to obtain the stable behavior, from which the information about d_1, d_2, and d_3 can be extracted. In calculating the saltation matrix S_1, the switching function is $h_1(x) = k_p x_1 - k x_2$, so that the normal is $\partial h_1(x)/\partial x = [k_p \; -k]$ and the time derivative is $\partial h_1(x)/\partial t = 0$. Similarly, for calculating S_2, the expression for the switching function is simply derived from (19) as $h_2(x) = k x_2 - (k_p x_1 - \Delta)$. Thus, $\partial h_2(x)/\partial x = [-k_p \; k]$ and $\partial h_2(x)/\partial t = 0$. With these expressions, we can obtain the saltation matrices

$$S_1 = I + \frac{(f_2^+ - f_1^-)\frac{\partial h_1(x)}{\partial x}}{\frac{\partial h_1(x)}{\partial x} f_1^- + \frac{\partial h_1(x)}{\partial t}} \; , \; S_2 = I + \frac{(f_3^+ - f_2^-)\frac{\partial h_2(x)}{\partial x}}{\frac{\partial h_2(x)}{\partial x} f_2^- + \frac{\partial h_2(x)}{\partial t}}$$

which are evaluated as

$$S_1 = \begin{bmatrix} 1 & 0 \\ -k_p a_1 & 1 + k a_1 \end{bmatrix}, \; S_2 = \begin{bmatrix} 1 - k_p a_2 & k a_2 \\ -k_p a_3 & 1 + k a_3 \end{bmatrix} \qquad (30)$$

where

$$a_1 = \frac{V_{in}/L}{\left(\frac{k_p}{RC} + \frac{k}{L}\right) V_{ref} - \frac{k}{L} V_{in} - \left(\frac{k_p}{RC} + \frac{k}{L}\right) x_1 + \left(\frac{rk}{L} - \frac{k_p}{C}\right) x_2}$$
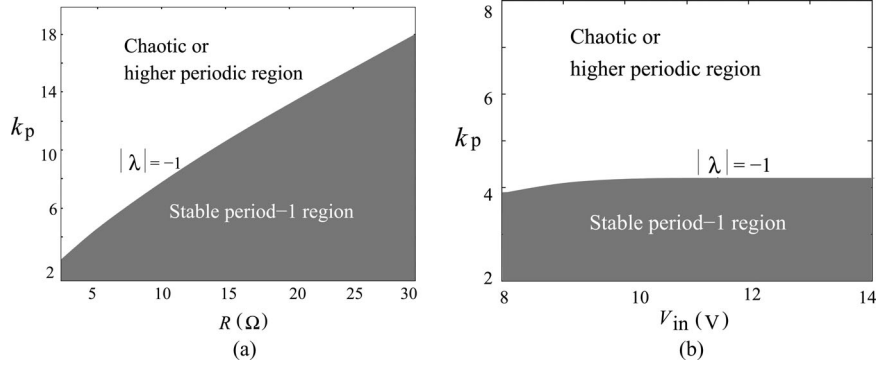
Fig. 10. Stability region of the period-1 orbits: (a) in R–k_p and (b) in V_{in}–k_p parameter space. The contours are obtained using the condition that the lower eigenvalue of the monodromy matrices W is equal to -1.

$$a_2 = \cfrac{x_2/C}{\left(\frac{k_p}{RC} + \frac{k}{L}\right)x_1 - \left(\frac{k_p}{RC} + \frac{k}{L}\right)V_{\text{ref}} - \left(\frac{rk}{L} - \frac{k_p}{C}\right)x_2}$$

$$a_3 = \cfrac{(V_{\text{ref}} - x_1)/L}{\left(\frac{k_p}{RC} + \frac{k}{L}\right)x_1 - \left(\frac{k_p}{RC} + \frac{k}{L}\right)V_{\text{ref}} - \left(\frac{rk}{L} - \frac{k_p}{C}\right)x_2}$$

and S_3 is an identity matrix. Note that the form of the monodromy matrix is sufficiently general. If the orbit contains passage through more number of subsystems with a number of crossings (for example, in a higher periodic orbit), one just has to compose the monodromy matrix out of the state transition matrices for the passage through each subsystem and the saltation matrices related to the crossings. This will greatly simplify the analysis as each crossing can be treated separately. Furthermore, the monodromy matrix essentially represents the linearized system integrated around the periodic orbits and hence their eigenvalues $\lambda_{1,2}$ represent the Floquet multipliers. If they lie within the unit circle, the orbit is stable. For example, if we choose the parameters $V_{\text{in}} = 12$ V, $L = 0.2$ mH, $C = 100$ μF, $T = 2$ μs, $k_p = 5.5$, $\Delta = 0.001$, $V_{\text{ref}} = 5$ V, and $R = 7.06$ Ω, then the corresponding duty ratios are found to be 0.2496, 0.3718, 0.3786, and the eigenvalues of the monodromy matrix -0.996 and 0.2848 are inside the unit circle. Therefore, the orbit is stable. Once it is stable, average dynamics will be zero value.

This provides a simple way for the circuit designer to choose the parameters for successful operation of SMC. Given certain specifications of v and power throughput, the designer would first roughly set the range of parameters in a conventional way based on Utkin's theory. This gives the desired slow time scale stability and transient performance, but will not guarantee that the system will be stable on a fast time scale when variable parameters like input voltage and load resistance fluctuate. In order to ensure the nominal period-1 operation, it will be necessary to calculate the range of the variable parameters for which the period-1 orbit will remain stable. A representative parameter space diagram of the FFHC-controlled converter is shown in Fig. 10(a) and (b). The designer will have to ensure that the external parameters remain within the shaded region of the parameter space. Once it is ensured, the solution of equivalent motion (6) always exists.

C. Equivalent Control and Equation of Motions

The equivalent control $u_{\text{eq}} \in (u_{1\text{eq}}, u_{2\text{eq}})$ is a means of finding the system motion restricted to the switching manifolds $h_i(x) = 0$ $(i = 1, 2, 3)$, and it can be determined by applying the invariance conditions $h_i(x) = 0$, $\partial h_i(x)/\partial x = 0$ [17], [35] if the average hysteretic flow of impinging vector fields $f_1(x)$, $f_2(x)$, and $f_3(x)$ with their associated time duration $u_{1\text{eq}}$, $(1 - u_{1\text{eq}} - u_{2\text{eq}})$, and $u_{2\text{eq}}$ are tangent to the SSs. Therefore, the dynamics within the quasi-stationary switching box can be described by the state-space averaged model

$$\frac{dx}{dt} = [A_1 x + B_1] u_{1\text{eq}} + [A_2 x + B_2] (1 - u_{1\text{eq}} - u_{2\text{eq}})$$
$$+ [A_3 x + B_3] u_{2\text{eq}} \tag{31}$$

where $u_{1\text{eq}}, u_{2\text{eq}} \in (0, 1)$. Further substitution of (9)–(11) into (31) yields

$$\frac{dx_1}{dt} = \frac{(V_{\text{ref}} - x_1)}{RC} - \frac{x_2}{C}(1 - u_{2\text{eq}})$$
$$\frac{dx_2}{dt} = -\frac{(V_{\text{ref}} - x_1)}{L}(1 - u_{2\text{eq}}) - \frac{rx_2}{L} + \frac{V_{\text{in}}}{L}u_{1\text{eq}}. \tag{32}$$

Here, it is important to point out that the discontinuous control inputs u_1 and u_2 have been replaced by their equivalent continuous controls $u_{1\text{eq}}$ and $u_{2\text{eq}}$, where the corresponding dynamics of $dx/dt = f_{\text{eq}}(x)$ is essentially composed of three subsystem equations. The derivation of such averaged dynamics of a PWM-controlled dc–dc converter operated in DCM has been reported by Sun *et al.* [36]. Based on this concept, the equivalent dynamics of the FFHC-controlled dc–dc converter can be obtained in full-order form as

$$\frac{dx_1}{dt} = \frac{(V_{\text{ref}} - x_1)}{RC} - \frac{(x_2 - I_0)}{C}$$
$$\frac{dx_2}{dt} = \frac{-2(V_{\text{ref}} - x_1)(x_2 - I_0)}{u_{1\text{eq}}T[V_{\text{in}} - (V_{\text{ref}} - x_1)]} + \frac{V_{\text{in}}}{L}u_{1\text{eq}} \tag{33}$$

where $r \approx 0$, $u_{1\text{eq}} \in (0, v/V_{\text{in}})$ and I_0 is the dc-offset value of inductor current due to M_3 operation. In (33), when $u_{1\text{eq}} \to 0$, both $x_2 \to I_0$ and $dx_2/dt \to 0$, getting a reduced-order system M_3 defined by $x_2 = I_0$ and $Cdx_1/dt = (V_{\text{ref}} - x_1)/R$.

Therefore, to conclude the analysis and the controller design, the stability of the converter system should be shown. A

generic system, described by $dx/dt = f(x)$ as (33) and whose Jacobian matrix at the equilibrium point $x_{ss} = (V_{ref} - V, \; I)$ (where $U_{1eq} \approx V_{ref}/V_{in}$ and $I_0 = k_p(V_{ref} - V) - \Delta$), which is denoted as $(D_f)|_{x_{ss}}$, is asymptotically stable if the eigenvalues $\lambda_{1,2}^s$ have negative real part [37]. That leads to solving the characteristics equation given by

$$\lambda^{s2} + (J_{11} + J_{22})\lambda^s + (J_{11}J_{22} - J_{12}J_{21}) = 0 \qquad (34)$$

where coefficients J_{11}, J_{12}, J_{21}, and J_{22} are shown in the Appendix. A criterion to choose the value for k_p could be to design the eigenvalues in order to make them coincide on the real axis [5]. However, to achieve the best dynamic responses, the system should evolve in steady state like a second-order system with a damping factor $\xi = 1$. In essence, the existence conditions (25) and (26), and the stability conditions derived from the monodromy matrix (29) form the basis for the selection to design the control gains of the proposed SM current controller (35) in terms of the converters specification. Satisfaction of these conditions assures the closed-loop stability of the system.

V. EXPERIMENTAL RESULTS

A. Experimental Validation of Theoretical Results

To verify the derived fixed-frequency MSSs based SM controller (see Fig. 11), we have implemented the system experimentally. The parameters used in the experiment setup are: $L = 1.80$ mH, $C = 72$ μF, $r = 0.01$ Ω, $\Delta = 0.2$, $T = 100$ μs, $k = 1$, $V_{ref} = 5$ V, and $V_{in} = 10$ V. Keeping the constraint of FFHC controller in mind (see Section IV), we have investigated fast-scale dynamics of the converter system under different parameter values. Fig. 12(a) shows that for $k_p = 8$ and $R = 3$ Ω, the converter operates in period-1 mode, so that the long-time average value of fast-scale chattered dynamics is zero. The application of equivalent SM control is therefore valid. However, as we change the parameter value to $k_p = 2$ and $R = 12$ Ω, the converter operates in a high periodic or chaotic region as shown in Fig. 12(b), which is inside the domain of chaotic attractor described in 2-parameter bifurcation (see Fig. 10). Although the proposed controlled converter exhibits fast-scale oscillations beyond certain parameter ranges, still its stable period-1 operating zone is quite a bit larger than the classical peak current-mode (PCM) controlled converter without slope compensation (SC). For a chosen value of $k_p = 3.5$ [satisfying inequality (27)], Fig. 10 shows that the FFHC-controlled converter can operate in nominal period-1 mode for parameters range $\{8 \text{ V} \leq V_{in} \leq 14 \text{ V}\}$ and $\{2.5 \text{ }\Omega \leq R \leq 30 \text{ }\Omega\}$. Whereas PCM controller shows its fast-scale instability when input voltage is approximately less than 10 V.

Therefore, in order to extract the best optimized performance, the FFHC controller gain k_p is optimally tuned using the approach proposed in (34) and (29) to give the fastest critically damped response ensuring the SM controller existence condition.
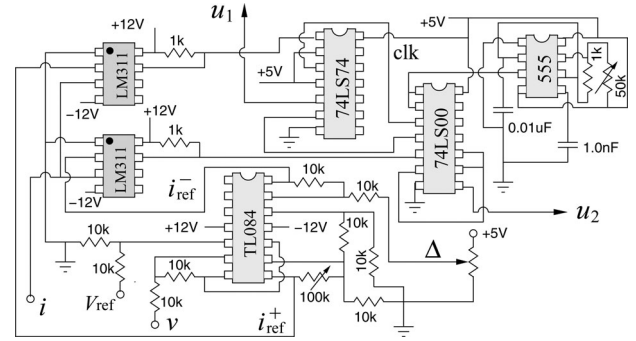

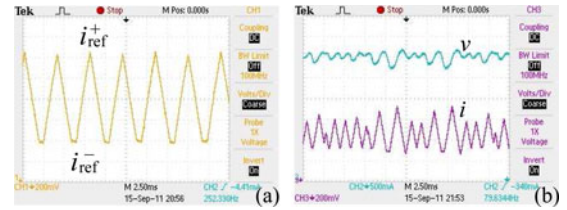Fig. 11.   Hardware realization of the proposed controller.

Fig. 12.   Experimental waveforms of the FFHC-controlled tristate buck converter showing (a) nominal period-1 operation for $k_p = 8$ and $R = 3$ Ω and (b) chaotic operation for $k_p = 2$ and $R = 12$ Ω.

B. Performance Comparison

Based on this principle, the performance of the proposed FFHC-controlled buck converter is experimentally verified and compared with conventional PMC-controlled buck converter without SC as shown in Fig. 13. The PCM controller without SC is known to exhibit faster transient response than other commonly used controllers such as voltage-mode or PCM controller with compensating ramp. The excellent system response under PCM controller (without SC), however, shows steady-state oscillatory behaviors when the converter operates for $d > 0.5$. Hence, it limits the application of this technique. To eliminate this instability, the use of SC technique again makes the system sluggish, and may even be unable to solve the problem especially for three-mode current-controlled converter. The addition of compensating ramp may also lead to instability through different mechanism [28]. The proposed control scheme takes less than one clock (≤ 100 μs) to settle under load fluctuation, which is approximately the same as that of the classical PCM controller without SC. Moreover under the same condition, it suffers from subharmonic oscillations. Fig. 13(b) and (c) shows the experimental proof of transient performance due to step change in load resistance from 3 Ω to 6 Ω and back to 3 Ω for $k_p = 8$. Similarly, the dynamic response of the FFHC controller is studied to see the effect of step change in the input voltage for $R = 2$ Ω. Fig. 13(d) and (e) shows the response of the system under step change in input voltage from 8 to 14 V, and back to 8 V. In both the cases, the controller acts as fast as the reference one without pushing the system into the unstable zone.

These optimized performances (in terms of stability and dynamic behaviors) of the proposed controlled converter therefore can meet the requirement of stable, fast-response regulated power supplies for the ever-increasing demands by next generation microprocessor load.
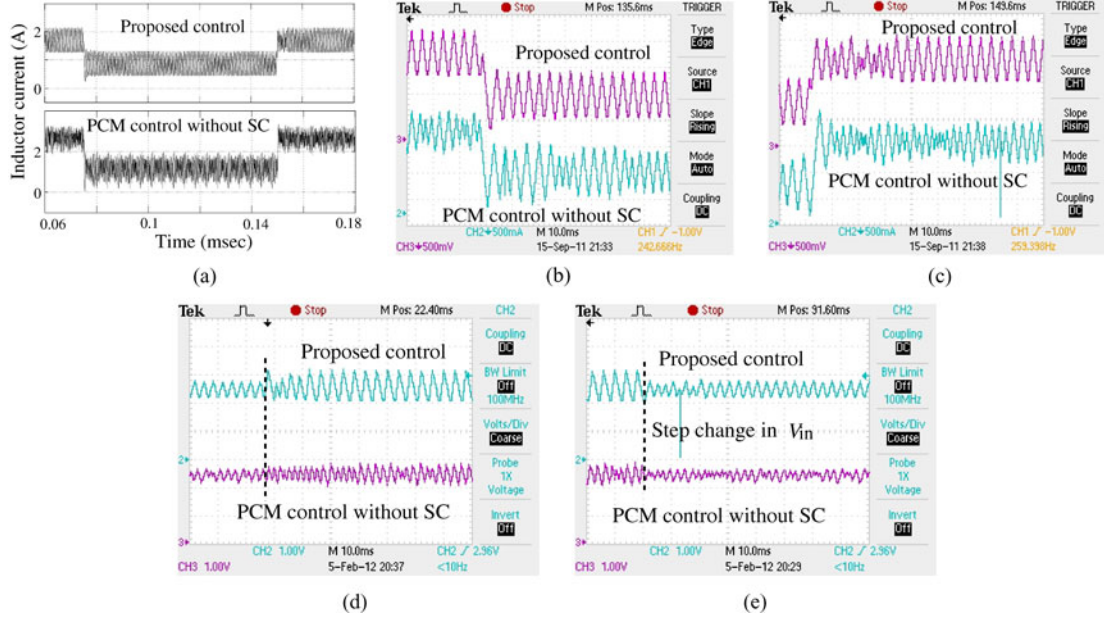
Fig. 13. Comparison of (a) simulation and experimental inductor current waveforms between the proposed FFHC-controlled tristate buck converter and the conventional PCM-controlled buck converter without SC under (b) step load change 3 to 6 Ω; and (c) 6 to 3 Ω, and input voltage change (d) 8 to 14 V, and (e) 14 to 8 V, respectively. The simulated results show the inductor current response due to change of step load resistance from 3 to 6 Ω and back to 3 Ω.

VI. Conclusion

In this paper, MSSs based fixed-frequency SM controller is proposed for buck-type converters. Based on the condition of SM in a multiscale HDS, we have derived the mathematical model of the system and showed that it yields an HDS with two-scale oscillations. Then, various aspects of the system such as the method of generating MSSs, the existence and stability properties, and the selection of the control parameters are discussed. It is shown that equivalent control based SMC design is only valid when the converter operates in periodic mode. We also addressed how both Filippov's method and Utkin's equivalent control law together can be used to design and extract its best optimized performance. Finally, its performance is experimentally verified and compared with PCM-controlled buck converter (without SC). The results demonstrate that, over a wide range of operating conditions, (i.e., wide variation of input voltage and load resistance) the transient response of the FFHC controller is as good as the reference one, without any subharmonic oscillations. It can therefore be concluded that the proposed FFHC controller may be a good alternative to conventional PCM (without SC) controller to achieve optimized performance with a low implementation cost and circuit complexity. However, investigations on efficiency and losses calculation under different loading conditions of such controlled system are still necessary and we are currently at work on that.

Appendix

To obtain the Jacobian matrix of (33), let us consider $g_1 = \frac{(V_{\text{ref}} - x_1)}{RC} - \frac{(x_2 - I_0)}{C}$ and $g_2 = \frac{-2(V_{\text{ref}} - x_1)(x_2 - I_0)}{u_{1\text{eq}}T[V_{\text{in}} - (V_{\text{ref}} - x_1)]} + \frac{V_{\text{in}}}{L}u_{1\text{eq}}$, where equivalent control input $u_{1\text{eq}}$ can be derived using (5) when $h(x) = h_1(x)$. By substituting the result into (33) and applying $dh_1(x)/dt = 0$, it can be obtained from (9) and (10)

as

$$u_{1\text{eq}} = \frac{\left(\frac{k_p}{RC} + \frac{k}{L}\right)(V_{\text{ref}} - x_1) - \frac{k_p}{C}x_2}{kV_{\text{in}}/L}. \quad (35)$$

Then, the linearization of (33) around the equilibrium points $(V_{\text{ref}} - V, I, U_{1\text{eq}})$ can be expressed as

$$\frac{d\tilde{x}}{dt} = \begin{pmatrix} \frac{\partial g_1}{\partial x_1} & \frac{\partial g_1}{\partial x_2} \\ \frac{\partial g_2}{\partial x_1} & \frac{\partial g_2}{\partial x_2} \end{pmatrix}\tilde{x} + \begin{pmatrix} \frac{\partial g_1}{\partial u_{1\text{eq}}} \\ \frac{\partial g_2}{\partial u_{1\text{eq}}} \end{pmatrix}\begin{pmatrix} \frac{\partial u_{1\text{eq}}}{\partial x_1} \\ \frac{\partial u_{1\text{eq}}}{\partial x_2} \end{pmatrix}^T \tilde{x} = \begin{pmatrix} J_{11} & J_{12} \\ J_{21} & J_{22} \end{pmatrix}\tilde{x}$$

where

$$\frac{\partial g_1}{\partial x_1} = -\frac{1}{RC}, \quad \frac{\partial g_1}{\partial x_2} = -\frac{1}{C}, \quad \frac{\partial g_2}{\partial x_1} = \frac{2(I - I_0)V_{\text{in}}}{U_{1\text{eq}}T(V_{\text{in}} - V)^2}$$

$$\frac{\partial g_2}{\partial x_2} = \frac{-2V}{U_{1\text{eq}}T(V_{\text{in}} - V)}, \quad \frac{\partial g_1}{\partial u_{1\text{eq}}} = 0$$

$$\frac{\partial g_2}{\partial u_{1\text{eq}}} = \frac{V_{\text{in}}}{L} + \frac{2V(I - I_0)}{U_{1\text{eq}}^2 T(V_{\text{in}} - V)}, \quad \frac{\partial u_{1\text{eq}}}{\partial x_1} = \beta_1, \quad \frac{\partial u_{1\text{eq}}}{\partial x_2} = \beta_2.$$

Here $\beta_1 = -\frac{k_p/RC + k/L}{kV_{\text{in}}/L}$ and $\beta_2 = -\frac{k_p/C}{kV_{\text{in}}/L}$. Substituting these values into the aforementioned equation yields

$$J_{11} = -\frac{1}{RC}, \quad J_{12} = -\frac{1}{C}$$

$$J_{21} = \frac{\beta_1 V_{\text{in}}}{L} + \frac{2(I - I_0)V_{\text{in}}}{U_{1\text{eq}}T(V_{\text{in}} - V)^2} + \frac{2\beta_1 V(I - I_0)}{U_{1\text{eq}}^2 T(V_{\text{in}} - V)}$$

$$J_{22} = \frac{\beta_2 V_{\text{in}}}{L} - \frac{2V}{U_{1\text{eq}}T(V_{\text{in}} - V)} + \frac{2\beta_2 V(I - I_0)}{U_{1\text{eq}}^2 T(V_{\text{in}} - V)}.$$

References

[1] International Technology Roadmap for Semiconductor. (2003). [Online]. Available: http:// www. public.itrs.net

[2] M. T. Zhang, M. M. Jovanovic, and F. C. Lee, "Design considerations for low-voltage on-board DC-DC modules for next generations of data processing circuits," *IEEE Trans. Power Electron.*, vol. 11, no. 2, pp. 328–337, Mar. 1996.

[3] R. W. Erickson and D. Maksimovic, *Fundamentals of Power Electronics*. New York: Springer-Verlag, 2000.

[4] F. L. Luo and H. Ye, "Small-signal analysis of energy factor and mathematical modeling for power dc-dc converters," *IEEE Trans. Power Electron.*, vol. 22, no. 1, pp. 69–79, Jan. 2007.

[5] R. D. Middlebrook and S. Cúk, "A general unified approach to modeling switching converter power stages," in *Proc. IEEE Power Electron. Spec. Conf.*, Cleveland, OH, 1976, pp. 18–34.

[6] C. K. Tse, *Complex Behavior of Switching Power Converters*. Boca Raton, FL: CRC Press, 2003.

[7] S. Banerjee and G. C. Verghese, Eds., *Nonlinear Phenomena in Power Electronics: Attractors, Bifurcations, Chaos, and Nonlinear Control*. Piscataway, NJ: IEEE Press, 2001.

[8] J. G. Kassakian, M. F. Schlecht, and G. C. Verghese, *Principles of Power Electronics*. New York: Addison-Wesley, 1991.

[9] M. López, L. G. Vicuña, M. Castilla, O. López, and J. Majó, "Interleaving of parallel dc-dc converters using sliding mode control," in *Proc. IEEE Ind. Electron. Soc.*, 1998, vol. 2, pp. 1055–1059.

[10] E. Figueres, G. Gercera, J. M. Benavent, M. Pascual, and J. A. Martinez, "Adaptive two-loop voltage-mode control of dc-dc switching converters," *IEEE Trans. Ind. Electron.*, vol. 53, no. 1, pp. 239–253, Feb. 2006.

[11] S. K. Mazumder, A. H. Nayfeh, and A. Boroyevic, "Robust control of parallel dc-dc buck converters by combining integral-variable-structure and multiple-sliding-surface control schemes," *IEEE Trans. Power Electron.*, vol. 17, no. 3, pp. 428–437, May 2002.

[12] S. C. Tan, Y. M. Lai, C. K. Tse, L. M. Salamero, and C. K. Wu, "A fast-response sliding-mode controller for boost-type converters with a wide range of operating conditions," *IEEE Trans. Ind. Electron.*, vol. 54, no. 6, pp. 3276–3286, Dec. 2007.

[13] A. Lachichi, S. Pierfederici, J. P. Martin, and B. Davat, "Study of a hybrid fixed frequency current controller suitable for dc-dc applications," *IEEE Trans. Power Electron.*, vol. 23, no. 3, pp. 1437–1448, May 2008.

[14] S. C. Tan, Y. M. Lai, and C. K. Tse, "Implementation of pulse-width-modulation based sliding mode controller for boost converters," *IEEE Power Electron. Lett.*, vol. 3, no. 4, pp. 130–135, Dec. 2005.

[15] Y. Chen and Y. Kang, "The variable-bandwidth hysteresis-modulation sliding-mode control for the PWM-PFM converters," *IEEE Trans. Power Electron.*, vol. 26, no. 10, pp. 2727–2734, Oct. 2011.

[16] S. Guo, X. L. Shi, B. Allard, Y. Gao, and Y. Ruan, "Digital sliding-mode controller for high-frequency dc/dc SMPS," *IEEE Trans. Power Electron.*, vol. 25, no. 5, pp. 1120–1123, May 2010.

[17] V. I. Utkin, Ed., *Sliding Modes and Their Application in Variable Structure Systems*. Moscow, Russia: MIR, 1978.

[18] J. W. Kimball, P. T. Krein, and Y. Chen, "Hysteresis and delta modulation control of converters using sensorless current mode," *IEEE Trans. Power Electron.*, vol. 21, no. 4, pp. 1154–1158, Jul. 2006.

[19] M. di. Bernardo, C. J. Budd, A. R. Champneys, and P. Kowalczyk, *Piecewise-smooth Dynamical Systems: Theory and Applications*. Applied Mathematical Sciences: New York: Springer, 2008.

[20] J. C. Alexander and T. I. Seidman, "Sliding modes in intersecting switching surfaces II: Hysteresis," *Houston J. Math.*, vol. 25, no. 1, pp. 185–211, 1999.

[21] S. C. Wong, X. Wu, and C. K. Tse, "Sustained slow-scale oscillation in higher order current-mode controlled converter," *IEEE Trans. Circuits Syst.-II*, vol. 55, no. 5, pp. 489–493, May 2008.

[22] Y. Chen, C. K. Tse, S. S. Qiu, L. Lindenmüller, and W. Schwarz, "Co-existing fast-scale and slow-scale instability in current-mode controlled dc/dc converters: Analysis, simulation and experimental results," *IEEE Trans. Circuits Syst.-I*, vol. 55, no. 5, pp. 3335–3348, Nov. 2008.

[23] S. K. Mazumder, A. H. Nayfeh, and D. Boroyevich, "Theoretical and experimental investigation of the fast-scale and slow-scale instabilities of a dc-dc converter," *IEEE Trans. Power Electron.*, vol. 16, no. 2, pp. 201–216, 2001.

[24] A. F. Filippov, *Differential Equations With Discontinuous Righthand Sides*. Dordrecht, The Netherlands: Kluwer, 1988.

[25] J. C. Alexander and T. I. Seidman, "Sliding modes in intersecting switching surfaces I: Blending," *Houston J. Math.*, vol. 24, no. 3, pp. 545–569, 1998.

[26] D. Ma and W. H. Ki, "Fast-transient PCCM switching converter with freewheel switching control," *IEEE Trans. Circuits Syst.-II*, vol. 54, no. 9, pp. 825–829, Sep. 2007.

[27] G. C. Verghese, M. E. Elbuluk, and J. G. Kassakian, "A general approach to sampled-data modeling for power electronic circuits," *IEEE Trans. Power Electron.*, vol. PE-1, no. 2, pp. 76–89, Apr. 1986.

[28] C. C. Fang, "Unified discrete-time modeling of buck converter in discontinuous mode," *IEEE Trans. Power Electron.*, vol. 26, no. 8, pp. 2335–2342, Aug. 2011.

[29] D. Giaouris, S. Banerjee, B. Zahawi, and V. Pickert, "Stability analysis of the continuous-conduction-mode buck converter via Filippovs method," *IEEE Trans. Circuits Syst.-I*, vol. 55, no. 4, pp. 1084–1096, May 2008.

[30] S. C. Tan, Y. M. Lai, C. K. Tse, and M. K. H. Cheung, "A fixed-frequency pulsewidth modulation based quasi-sliding-mode controller for buck converters," *IEEE Trans. Power Electron.*, vol. 20, no. 6, pp. 1379–1392, Nov. 2005.

[31] Z. T. Zhusubaliyev, E. Mosekilde, and O. O. Yanochkina, "Torus-bifurcation mechanisms in a dc/dc converter with pulsewidth-modulated control," *IEEE Trans. Power Electron.*, vol. 26, no. 4, pp. 1270–1279, Apr. 2011.

[32] S. Maity, D. Tripathy, T. K. Bhattacharya, and S. Banerjee, "Bifurcation analysis of PWM-1 voltage-mode controlled buck converter using the exact discrete model," *IEEE Trans. Circuits Syst.-I*, vol. 54, no. 5, pp. 1120–1130, May 2007.

[33] R. I. Leine and H. Nijmeijer, *Dynamics and Bifurcations of Non-Smooth Mechanical Systems*. New York: Springer, 2004.

[34] D. Giaouris, S. Maity, S. Banerjee, V. Pickert, and B. Zahawi, "Application of Filippov method for the analysis of subharmonic instability in dc-dc converters," *Int. J. Circuit Theory Appl.*, vol. 37, no. 8, pp. 899–919, 2009.

[35] H. S. Ramirez, "Differential geometric methods in variable-structure control," *Int. J. Control*, vol. 48, no. 4, pp. 1359–1390, 1988.

[36] J. Sun, D. M. Mitchell, M. F. Greuel, P. T. Krein, and R. M. Bass, "Averaged modeling of PWM converters operating in discontinuous conduction mode," *IEEE Trans. Power Electron.*, vol. 16, no. 4, pp. 482–492, Jul. 2001.

[37] B. C. Kuo, *Automatic Control Systems*. Hoboken, NJ: Wiley, 2002.

Somnath Maity (M'11) received the M.Tech degree from the Indian Institute of Technology, Madras, India, in 2003, and the Ph.D. degree from the Indian Institute of Technology, Kharagpur, West Bengal, India, in 2009.

Presently, he is an Assistant Professor in the Department of Electrical Engineering, National Institute of Technology, Rourkela, Orrisa, India. His areas of research interest include nonlinear dynamics of power electronic circuits and systems, modeling and analysis of complex engineered systems such as smart grids, hybrid electric vehicles, and DC distributed power systems.

Y. Suraj was born in Kurnool, Andhra Pradesh, India on December 4, 1989. He received the B.Tech degree in electrical and electronics engineering from G. Pulla Reddy Engineering College, Kurnool, in 2010. He is currently working toward the M.Tech degree from the Department of Electrical Engineering, National Institute of Technology, Rourkela, Orissa, India. His research interests include power electronics and electrical drives.